Surgical Endoscopy (2022) 36:5121–5135
https://doi.org/10.1007/s00464-021-08882-4

Analyzing material changes consistent with degradation of explanted polymeric hernia mesh related to clinical characteristics

Xinyue Lu[1] · Melinda Harman[1] · B. Todd Heniford[2] · Vedra Augenstein[2] · Brittney McIver[1] · William Bridges[3]

Received: 17 August 2021 / Accepted: 16 November 2021 / Published online: 7 March 2022
© The Author(s), under exclusive licence to Springer Science+Business Media, LLC, part of Springer Nature 2022

Abstract

Background Proposed mechanisms that potentially contribute to polypropylene mesh degradation after in vivo exposure include oxidizing species and mechanical strains induced by normal healing, tissue integration, muscle contraction, and the immediate and chronic inflammatory responses.

Methods This study explores these potential degradation mechanisms using 63 mesh implants retrieved from patients after a median implantation time of 24 months following hernia repair surgery (mesh explants) and analysis of multivariate associations between the material changes and clinical characteristics. Specifically, polypropylene mesh degradation was characterized in terms of material changes in surface oxidation, crystallinity and mechanical properties, and clinical characteristics included mesh placement location, medical history and mesh selection.

Results Compared to pristine control samples, subsets of mesh explants had evidence of surface oxidation, altered crystallinity, or changed mechanical properties. Using multivariate statistical approach to control for clinical characteristics, infection was a significant factor affecting changes in mesh stiffness and mesh class was a significant factor affecting polypropylene crystallinity changes.

Conclusions Highly variable in vivo conditions expose mesh to mechanisms that alter clinical outcomes and potentially contribute to mesh degradation. These PP mesh explants after 0.5 to 13 years in vivo had measurable changes in surface chemistry, crystallinity and mechanical properties, with significant trends associated with factors of mesh placement, mesh class, and infection.

Keywords Polypropylene · Degradation · Reactive oxygen species (ROS) · Mechanical strain · Hernia · Mesh

Surgical guidelines recommend hernia mesh implants as the general standard for inguinal hernia repair [1]. In use since the 1950s, polypropylene (PP) biomaterials are common in commercially available hernia meshes due to their high tensile strength, good flexibility, and chemical resistance [2]. Although in vivo biomechanical and biochemical mechanisms have the potential to degrade biomaterials [3–8]; the extent of in vivo degradation of PP mesh implants is currently under debate [9–11]. Some studies of explanted PP mesh implants cite changes in chemical markers (e.g., surface oxidation and crystallinity) and physical markers (e.g., surface cracking and reduced compliance) as evidence of in vivo degradation of the PP mesh [6, 12–15]. Other studies of explanted PP mesh implants cite an absence of changes in chemical markers, most notably in PP formulated with antioxidant stabilizers, and attribute surface cracking to artifacts from formalin-fixed proteins adhered to the mesh surface [3, 10, 16]. Ineffective cleaning of explanted PP mesh [10] and highly variable clinical conditions, such as the presence of acute infection or chronic inflammation, further complicate these seemingly contradictory results [16].

There are several mechanisms that potentially contribute to PP mesh in vivo degradation. One proposed mechanism involves reactive oxygen species (ROS) and myeloperoxidase (MPO) that are present in cases of infection and chronic inflammation in peritoneal fluid [5, 17, 18]. These chemicals are capable of oxidizing PP mesh and causing radical

✉ Melinda Harman
harman2@clemson.edu

[1] Department of Bioengineering, Clemson University, Clemson, SC 29634, USA

[2] Gastrointestinal and Minimally Invasive Surgery, Carolinas Medical Center, Charlotte, NC 28204, USA

[3] Department of Mathematical Sciences, Clemson University, Clemson, SC 29634, USA

scission, and possibly leading to changes in crystallinity [5, 12, 15, 16, 19]. Another proposed mechanism involves sustained and cyclic mechanical strains in the mesh that exist during the surgical procedure and healing process and with patient activities after implantation [20–22]. Such strains are capable of increasing localized stress, initiating structural cracks in individual fibers, and causing polymer chain scission, which may contribute to PP degradation such as surface cracking, changes in crystallinity, and even mesh failure [7, 12, 20, 21]. The degraded PP may increase the inflammatory response around the implanted mesh, potentially increasing the concentrations of ROS and MPO and leading to further PP degradation [12].

Highly variable in vivo conditions expose a mesh to a mechanism that potentially contributes to PP mesh degradation and complicates the analysis of explanted PP mesh. Surgical placement of the mesh within the peritoneal cavity (intra-peritoneal location) results in mesh being in contact with peritoneal fluid. The peritoneal fluid actively exchanges leukocytes with blood [23] and contains increased ROS released from leukocytes or macrophages in cases of infection or chronic inflammation [17, 24], thus creating the chemical environment for PP degradation. Surgical injuries or infection are the triggers causing fibrosis or scar formation of the peritoneum, applying increased mechanical strain on implanted mesh for PP degradation [23]. Medical comorbidities, such as obesity [25], diabetes [26–28] and tobacco use [26] can alter and delay wound healing. These medical comorbidities can lead to chronic inflammation and abnormal tension applied on mesh, creating the chemical and mechanical environment for PP degradation.

Mesh selection also potentially contributes to PP mesh degradation. Mesh with small pore sizes has a larger surface contact area with host tissues, inducing higher inflammatory infiltrate to the mesh surface by attracting inflammatory cells, such as macrophages [29–31]. These inflammatory cells on the mesh surface release ROS, increasing the amounts of ROS around the mesh and creating the chemical environment for PP degradation. Mesh with small pore sizes also induces less tissue integration but higher fibrous encapsulation, leading to higher tissue contraction [22, 32–34]. This contraction applies mechanical strains on the mesh, creating a mechanical environment for PP degradation. Mesh with highly deformable pore shape can behave similarly to mesh with small pores under the biaxial tension caused by abdominal wall distension, healing process or tissue contraction [29, 35].

To date, few studies of explanted PP mesh have explored specific mechanisms that potentially contribute to PP mesh degradation. Evidence of degradation is confounded by contamination from chemical fixatives and adhered biological debris, highly variable in vivo conditions that are infrequently documented, and small sample sizes that are not suitable for meaningful statistical analysis. There is need for explant analysis of PP hernia mesh that centers on potential degradation mechanisms and investigates clinical characteristics that may trigger material changes consistent with PP degradation. The purposes of this study were: (1) to evaluate mesh surface oxidation, crystallinity, and mechanical properties of fresh frozen explanted PP meshes; and (2) to investigate whether material changes consistent with PP degradation are related to infection, mesh placement location, and mesh pore size. The initial hypothesis were: (1) meshes explanted from patients with infection have more PP material changes than meshes explanted from non-infected patients; (2) meshes implanted in an intra-peritoneal location have more PP material changes than meshes implanted in an extra-peritoneal location; and (3) meshes with small pore size have more PP material changes than meshes with large pore size. Based on detailed analysis, several sub-hypotheses also were considered.

Materials and methods

Materials

Hernia meshes were collected by the surgeon co-authors (BTH, VA) through an established registry of explanted meshes (MeshWatch) using a protocol approved by the Clemson University Institutional Review Board (IRB2014-161). Meshes from consecutive patients undergoing revision hernia surgery were archived and stored fresh-frozen at −80 °C until analysis. To date, there are 164 explanted hernia meshes of various types in the registry along with documentation of basic patient demographics and clinical history abstracted from available records and details of mesh structure and type. The registry database was queried to identify all meshes meeting five inclusion criteria. (1) The meshes were explanted by the same surgical team at the same medical center. (2) The mesh material was PP. (3) The meshes were received before the start of this study (December 2017). (4) The mesh structure was in the pictorial "MeshWatch" atlas of known mesh types in the mesh registry [36]. (5) The mesh structure was warp knitted. Sixty-three meshes of 10 known mesh structures met those inclusion criteria ($n = 63$) and were selected for further analysis.

The included meshes ($n = 63$) were explanted from 62 patients after a median implantation time of 24 (range: 5 to 156) months. There were 32 female patients (average age at removal: 57 ± 12 years old) and 30 male patients (average age at removal: 61 ± 11 years old), including two meshes retrieved from one male patient (Table 1). Patient records included sex, age at removal, BMI, and mesh implantation time. The year of mesh implantation (range: 2002 to 2016) into a patient was estimated using the year of mesh removal

Table 1 Patient information

Mesh #	Sex (F/M)	Age (years)	BMI	In vivo time (mons)	Mesh location	Infection (Y/N)	Removal reason	Smk/Dia/Pre hernia rep/Rec hernia (Y/N)
Class I								
1	F	49	29.3	48	Onlay	N	Incarcerated hernia	N/N/Y/Y
2	M	68	33.6	11	Onlay	N	Seroma	N/N/Y/Y
3	M	60	45.3	132	Onlay	Y	Infection	N/N/N/Y
4	F	68	28.6	9	Onlay	N	Incarcerated hernia	N/N/Y/Y
5	F	37	37.6	53	Onlay	N	Incarcerated hernia	N/Y/Y/Y
6	M	68	28.6	33	Onlay	N	Incarcerated hernia	N/N/Y/Y
7	F	60	45.0	24	Inlay	N	Sus rec hernia	N/Y/N/Y
8	F	58	30.9	7	Inlay	N	Sus rec hernia	N/N/Y/Y
9	F	48	39.1	8	Underlay	N	Sus rec hernia	Y/N/Y/Y
10	M	48	19.9	37	Underlay	N	Chronic pain	Y/N/N/Y
11	M	58	28.0	16	Underlay	N	Incarcerated hernia	N/N/N/Y
12	M	51	33.7	18	Underlay	Y	Infection	N/N/N/Y
13	M	51	33.7	18	Underlay	Y	Infection	N/N/N/Y
14	M	73	28.3	19	Sublay	N	Incarcerated hernia	N/N/Y/Y
15	F	51	40.2	5	Intra	Y	Infection	N/N/Y/Y
16	M	50	30.5	25	Intra	N	Sus rec hernia	N/N/N/Y
17	F	32	34.0	54	Intra	N	Incarcerated hernia	N/N/Y/Y
18	F	67	30.1	22	Intra	N	Incarcerated hernia	N/N/Y/Y
19	F	78	40.7	96	Intra	Y	Infection	N/N/Y/Y
20	M	57	29.9	9	Intra	N	Incarcerated hernia	N/N/Y/Y
21	F	56	32.9	48	Intra	N	Incarcerated hernia	N/N/N/Y
22	F	41	33.5	12	Intra	N	Sus rec hernia	N/N/Y/Y
Class II								
23	M	74	30.1	24	Onlay	N	Sus rec hernia	N/Y/Y/Y
24	F	41	35.3	24	Inlay	Y	Incarcerated hernia	N/N/Y/Y
25	M	63	44.3	8	Underlay	N	Incarcerated hernia	N/Y/N/Y
26	M	54	26.9	36	Underlay	N	Incarcerated hernia	N/N/Y/Y
27	M	70	29.2	12	Underlay	N	Incarcerated hernia	N/N/Y/Y
28	M	54	33.1	15	Underlay	N	Incarcerated hernia	N/N/Y/Y
29	F	34	38.1	30	Underlay	N	Incarcerated hernia	N/N/N/Y
30	M	60	32.3	14	Underlay	N	Incarcerated hernia	N/N/Y/Y
31	F	58	45.9	48	Underlay	N	Incarcerated hernia	N/N/Y/Y
32	F	64	25.0	11	Underlay	N	Seroma	N/N/N/Y
33	M	75	28.8	9	Sublay	N	Sus rec hernia	N/N/Y/Y
34	M	75	28.8	18	Sublay	N	Incarcerated hernia	N/N/N/N
35	M	71	47.3	48	Sublay	N	Incarcerated hernia	N/Y/Y/Y
36	F	52	40.3	13	Sublay	N	Sus rec hernia	N/Y/Y/NA
37	F	48	42.2	25	Intra	N	Sus rec hernia	Y/Y/Y/Y
38	F	65	36.7	15	Intra	N	Sus rec hernia	N/N/Y/Y
39	M	57	26.5	5	Intra	N	Sus rec hernia	N/N/N/Y
40	F	75	30.8	31	Intra	N	Mesh attachment	N/N/N/Y
41	F	65	26.7	50	Intra	N	Bowel obstruction	N/N/N/N
42	M	71	28.7	13	Intra	N	Diastasis	N/N/Y/Y
43	F	54	31.0	7	Intra	N	Fistula	N/N/Y/Y
44	F	61	29.5	28	Intra	Y	Incarcerated hernia	N/Y/Y/Y
45	M	50	28.7	NA	NA	NA	NA	Y/NA/NA/NA

Table 1 (continued)

Mesh #	Sex (F/M)	Age (years)	BMI	In vivo time (mons)	Mesh location	Infection (Y/N)	Removal reason	Smk/Dia/Pre hernia rep/Rec hernia (Y/N)
Class III								
46	F	58	35.5	29	Onlay	N	Incarcerated hernia	N/Y/Y/Y
47	F	68	31.5	156	Onlay	N	Incarcerated hernia	N/N/Y/Y
48	M	38	34.8	NA	Onlay	N	Sus rec hernia	N/N/Y/NA
49	M	75	28.3	15	Onlay	Y	Infection	N/Y/N/NA
50	M	69	28.0	9	Inlay	N	Incarcerated hernia	N/Y/Y/NA
51	M	44	34.4	13	Underlay	N	Chronic pain	N/N/N/N
52	F	64	41.6	18	Underlay	N	Incarcerated hernia	N/N/Y/NA
53	M	43	44.4	84	Sublay	N	Hard mesh	N/Y/Y/Y
54	F	54	48.9	NA	Sublay	N	Incarcerated hernia	N/N/Y/Y
55	M	65	36.0	34	Sublay	N	Incarcerated hernia	N/N/Y/Y
56	F	69	32.5	133	Intra	N	Sus rec hernia	N/Y/Y/Y
57	F	68	32.8	NA	Intra	N	Incarcerated hernia	N/Y/Y/Y
58	M	55	29.0	120	Intra	N	Incarcerated hernia	N/Y/Y/Y
59	M	64	28.5	28	Intra	N	Chronic pain	N/N/N/NA
60	F	42	50.5	96	Intra	N	Bowel obstruction	N/Y/Y/NA
61	F	65	34.3	41	Intra	N	Sus rec hernia	N/N/Y/Y
62	M	65	27.7	132	Intra	N	Sus rec hernia	N/N/Y/Y
63	F	58	29.5	84	Intra	NA	Adhesion	N/N/Y/Y

Age age at removal

Sus rec hernia suspected recurrent hernia

Smk patients with smoking history

Dia patients with diabetes

Pre hernia rep previous hernia repair

Rec hernia recurrent hernia

(range: 2013 to 2017) and the implantation time. Medical records included history of infection, diabetes, recurrent hernia, smoking and previous hernia repair. Surgical records included mesh placement and reasons for mesh removal. The reasons for mesh removal included infection ($n=8$), incarcerated hernia ($n=29$, two patients with both infection and incarcerated hernia), bowel obstruction ($n=2$), suspected recurrent hernia ($n=15$), chronic pain ($n=3$), and other individual issues ($n=7$). Some patients did not have full records: (1) Eight patients did not have records of recurrent hernia. (2) Four patients did not have records of implantation time. (3) Two patients did not have records of infection, including one patient who did not have a recorded history of mesh placement anatomic location, implantation time, diabetes, previous hernia repair, and reasons for removal.

Using the data of medical records, the included meshes were grouped into meshes from infected patients ($n=8$) and meshes from non-infected patients ($n=53$). Based on the comorbidities, the included meshes were grouped into meshes from patients with diabetes ($n=16$) and without diabetes ($n=46$), with previous hernia repair ($n=44$) and without previous hernia repair ($n=18$), with recurrent hernia ($n=52$) and without recurrent hernia ($n=3$), and with a history of smoking ($n=4$) and without a history of smoking ($n=59$).

According to surgical records, the included meshes were grouped into two anatomic locations based on mesh placement before retrieval: intra-peritoneal (Intra) location ($n=24$) and extra-peritoneal (Extra) location ($n=38$). The extra-peritoneal location included four anatomic locations: onlay ($n=11$), inlay ($n=4$), underlay ($n=15$), and sublay ($n=8$) [37].

According to mesh selection, the included meshes were classified into three groups based on modified Klinge's classification: Class I ($n=22$) were large pore meshes (textile porosity > 60%); Class II ($n=23$) were small pore meshes (textile porosity < 60%); and Class III ($n=18$) were meshes with special features, such as barrier layer or surface coating (Table 2) [38]. For the explanted meshes, the presence of an absorbable surface coating at the time of implantation could not be traced and therefore, only meshes with an e-PTFE layer were classified into Class III. All other meshes were

Table 2 Mesh structures (scale bar: 1000 µm)

Class I (n = 22)	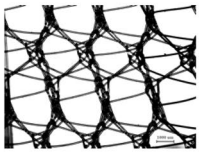	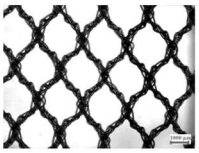	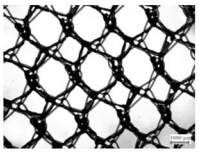	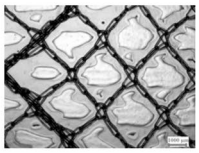
Class II (n = 23)	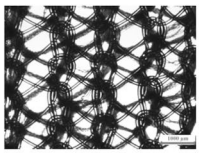	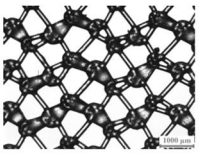		
Class III (n = 18)	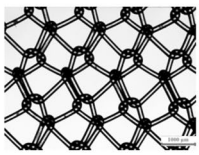	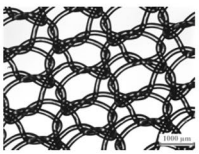	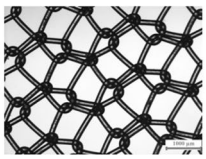	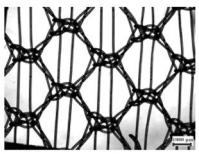

classified into Class I or Class II based on the porosity. Two Class III mesh microscope images were similar but their overall shapes were different. Overall, the mesh explants represented 10 mesh structures of nine different commercially available mesh types.

Methods

Explanted mesh handling

The explanted meshes were handled carefully. Selected explanted meshes were thawed to room temperature and carefully flattened. Two mesh samples with 2 cm × 2 cm region of interest were cut for chemical and mechanical characterization. Mesh samples were rinsed with 0.02 M phosphate buffer solution (PBS) to remove excessive blood.

Mesh sample cleaning

The adhered tissues on the mesh samples were carefully removed using a 10-step modified cleaning protocol to avoid interference with subsequent analysis methods (Table 3) [10]. Tissues were enzymatically removed by immersing in 1.5% NSPO034 protease solution (Novozymes, Bagsværd, Denmark) and 1.5% Alcalase 2.5 L (Novozymes, Bagsværd, Denmark) in 0.02 M phosphate buffer (pH = 7) at 50 °C for 24 h, followed by 0.5% detergent (Novozymes, Bagsværd, Denmark) bath at 80 °C for 30 min. The tissue residues on mesh samples were further removed using fresh enzymatic solution and then fresh detergent solution for 2 h, respectively, at 50 °C in ultrasonic bath. The enzyme and detergent residues were rinsed off by Millipore water in ultrasonic bath at 50 °C for 2 h. Mesh samples were disinfected by soaking in 70% ethanol for 1 min and rinsed in Millipore water and vacuum dried at ambient temperature for chemical and mechanical characterization. Commercially available unused pristine meshes were processed as cleaned controls.

Cleaning validation

Validation of cleaned mesh samples included visual assessment under a stereo optical microscope (SMZ-168, Motic, Richmond, Canada) and chemical assessment with

Table 3 Mesh sample cleaning protocol

Step 1	Step 2	Step 3	Step 4	Step 5
Remove blood using PBS buffer	Digest tissues using enzyme solution at 50 °C for 24 h	Verify removal of tissues from mesh, Yes → step 4 No → step 2	Rinse and leave in 0.5% detergent at 80 °C for 30 min	Sonicate using fresh enzyme solution at 50 °C for 2 h
Step 6	**Step 7**	**Step 8**	**Step 9**	**Step 10**
Sonicate using fresh detergent solution 50 °C for 2 h	Rinse and sonicate in Millipore water 50 °C for 2 h	Disinfect in 70% ethanol for 1 min	Rinse using Millipore water	Vacuum dry before characterization

Fourier-transform infrared spectroscopy (FTIR) (IRSpirit FTIR Spectrometer, Shimadzu, Kyoto, Japan), similar to the validation method reported by Thames, et al. [10]. Mesh samples with remaining adhered tissues were not translucent and had 1600–1690 cm^{-1} spectral peaks in FTIR, whereas clean mesh samples were translucent and the 1600–1690 cm^{-1} spectral peaks were absent. Based on preliminary testing, mesh samples were cleaned using the cleaning protocol (Table 3) until little improvement was observed under the microscope and the peak representing proteins in the region of 1600–1690 cm^{-1} (Fig. 1a, red curve) was not observed under FTIR (Fig. 1a, blue curve). The peak in the region of 3300 cm^{-1} was not used as protein indicator because the range of 3100–3600 cm^{-1} also represented hydroxyl groups [10, 39].

Surface degradation characterization

Change in surface chemistry PP mesh surface degradation was characterized by detection of surface chemical changes on the cleaned mesh samples compared to pristine cleaned controls. Surface chemistry was measured using FTIR (IRSpirit FTIR Spectrometer, Shimadzu, Kyoto, Japan). The mesh surface was scanned in the range of 500 to 4000 cm^{-1} with resolution of 4 cm^{-1}. Compared to pristine PP mesh (Fig. 1b), the mesh samples without surface chemical changes (Fig. 1a, blue curve) had similar FTIR peaks, but mesh samples with surface chemical changes (Fig. 1a, green curve) had evidence of carbonyl groups (1740 cm^{-1}) [12, 19] or hydroxyl groups (3100–3600 cm^{-1}) [5, 19]. The observation of carbonyl groups confirmed the oxidation of the PP chain. The observation of hydroxyl groups confirmed the cross-linking of the hydrogen bonds to the PP chain [39].

Although some meshes had absorbable films before implantation, such as poliglecaprone (Fig. 1c), the peaks (580 cm^{-1}, 725 cm^{-1} and 1081 cm^{-1}) representing poliglecaprone film was not observed in explanted mesh samples, confirmed by FTIR (Fig. 1d) [40]. Explanted mesh sample #2 (Fig. 1d, red curve) and #7 (Fig. 1d, blue curve) were the same type mesh with absorbable materials (Fig. 1c) before implantation. Both mesh samples (Fig. 1d) were notably different from the pristine mesh samples with the intact absorbable layer (Fig. 1c) with reduction of peaks of 580 cm^{-1}, 725 cm^{-1} and 1081 cm^{-1}. Both mesh samples (Fig. 1d) had peaks similar as pristine PP mesh (Fig. 1b), confirming the observation of carbonyl groups (~1740 cm^{-1}) consistent with oxidative change in the PP surface chemistry.

Bulk degradation characterization

Change in crystallinity characterization PP mesh bulk degradation was characterized as the percent change in crystallinity for the cleaned explanted mesh samples compared to pristine cleaned controls. The degree of crystallinity was measured using differential scanning colorimetry (DSC) (Q1000 DSC Instrument, TA Instruments, New Castle, DE). The mesh samples were heated from 25 to 200 °C with heat rate of 20 °C/min. The degree of crystallinity (Xc) of the mesh samples was calculated from the tested heat of fusion (H_f) to the heat of fusion of 100% crystalline polypropylene ($H_{f,100}$), which equals 209 J/g [39].

$$Xc = H_f / H_{f,100\,(=209\,J/g)} \times 100\% \tag{1}$$

The change in crystallinity ($X_{c,changed}$) was determined by comparing to pristine cleaned controls ($X_{c,pristine}$).

$$X_{c,changed} = X_{c,explanted} - X_{c,pristine} \tag{2}$$

The percent change in crystallinity was normalized relative to the crystallinity of pristine cleaned controls.

$$X_{c,changed}\% = X_{c,changed} / X_{c,pristine} \times 100\% \tag{3}$$

Due to the limited dimension of one explanted mesh, 62 explanted meshes was characterized and generated crystallinity measures.

Change in stiffness characterization Indirect characterization of PP mesh bulk degradation was evaluated as a change in stiffness for the explanted mesh samples compared to pristine cleaned controls. Mesh stiffness was calculated from mechanical behavior measured using a biaxial tensile test (BioTester, CellScale, Ontario, Canada). The mesh samples were preconditioned by soaking in 1×PBS solution at 37 °C for 15 min. The hydrated mesh samples were clamped on the biaxial tester equipped with orthogonal 23 N load cells and a high-resolution CCD imaging system for image-based strain measurement, leaving a 2 cm×2 cm region of interest. Each test sample was preconditioned by 10 cycles of cyclic stretching at a speed of 0.2 mm/s with displacement of 5% tensile strain in both directions, followed by a stretching at the same speed to peak tension [35]. Due to the anisotropic behavior of some mesh samples, all tested samples were aligned according to the notable longitudinal (y-direction) and transverse directions (x-direction) [35]. The mesh stiffness Sx (N/cm) and mesh stiffness Sy (N/cm) were calculated as the slope of the linear region of the tension-strain curves. The percent change in stiffness ($S_{changed}\%$) was normalized relative to the stiffness of pristine mesh.

$$S_{changed}\% = (S_{explantedmesh\,sample} - S_{pristine\,mesh\,sample}) / S_{pristine\,mesh\,sample} \times 100\% \tag{4}$$

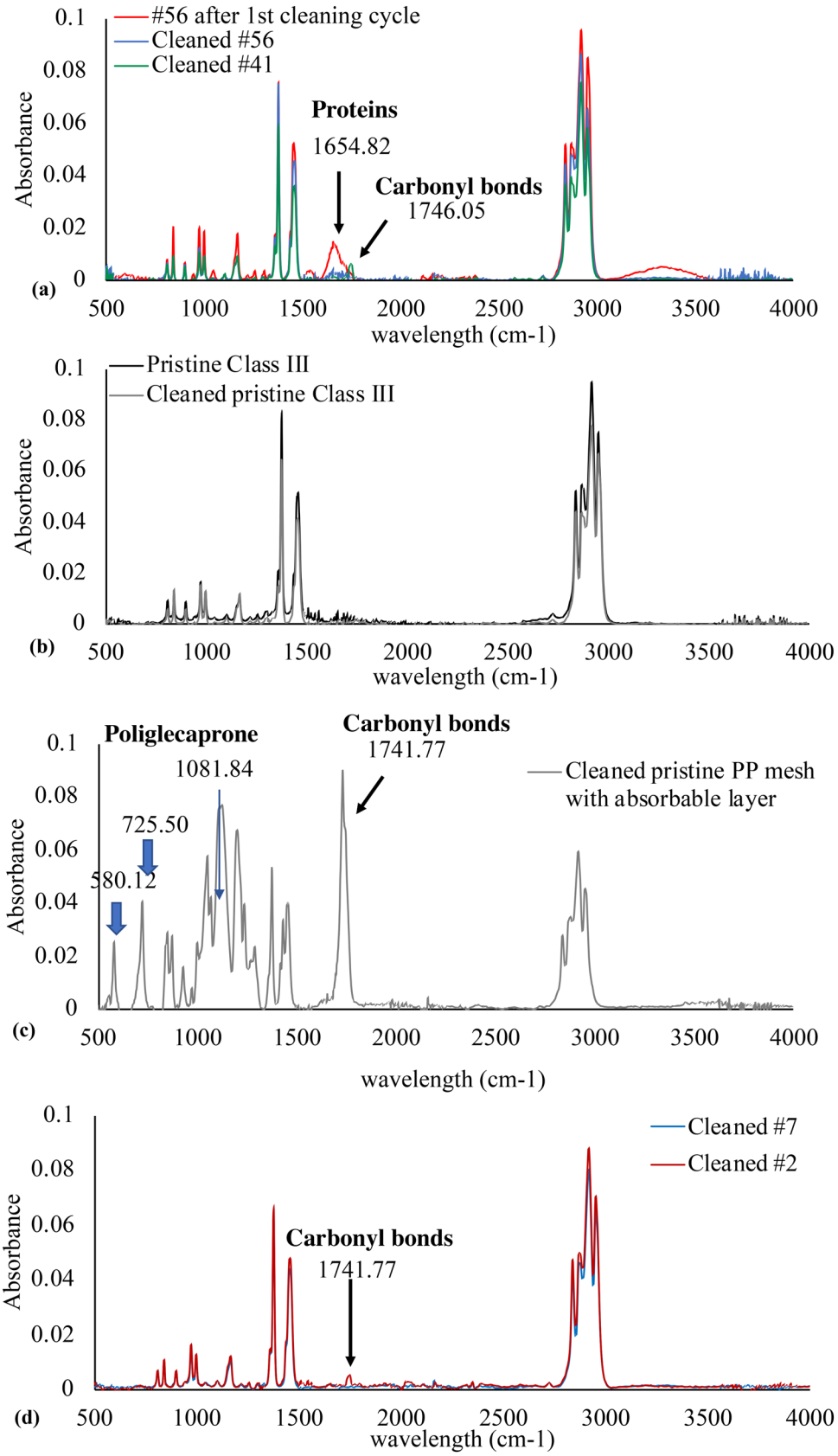

Fig. 1 FTIR of pristine and cleaned mesh samples. **a** FTIR of #56 after 1 cycle of 10-step cleaning (red) and after 2 cycles of cleaning (blue), compared to cleaned #41 (green) **b** FTIR of pristine (black) and cleaned pristine PP mesh (grey). **c** FTIR of cleaned pristine mesh with absorbable layer (grey) **d** FTIR of cleaned mesh samples after absorbance of absorbable layer #7 (blue) and #2 (red) after implantation (Color figure online)

Due to the limited dimensions of some explanted mesh samples, only 35 explanted meshes underwent mechanical testing and generated stiffness measures.

Statistical analysis [41]

The measured results were the dependent variables in the analyses, specifically the surface chemical changes ($C_{surface}$) (Y/N), the crystallinity changes ($X_{c,changed}$%) and the stiffness changes ($S_{changed}$%). The patient demographics, medical conditions, surgical location, and mesh classification (Table 4) were independent variables in the analyses. To address hypothesis 1, the bivariate relationship between each dependent variable and variable infection (Y/N) was tested. To address hypothesis 2, the bivariate relationship between each dependent variable and the mesh location (intra/extraperitoneal) was tested. To address hypothesis 3, the bivariate relationship between each dependent variable and mesh class (Class I, Class II, Class III) was tested.

Additional independent variables from patient and medical records such as sex (M/F), diabetes (Y/N), BMI, pervious hernia repair (Y/N), recurrent hernia (Y/N), smoking status (Y/N), implantation time (months), estimated year of implantation, and age at removal (years) were also used to (1) explore additional bivariate relationships between the dependent variables and independent variables not specifically addressed in the hypotheses; and (2) further test the relationships for the three hypotheses using all the independent variables and a multivariate generalized regression model.

Traditional statistical methods were used to test the bivariate relationships with attention to the nature of the variables (categorical or continuous) and the actual distributions (binomial or multinomial for categorical, normal or non-normal for continuous). The relationships between binomial dependent variables and binomial independent variables were analyzed with a Chi square test, or a Fisher's exact test, depending on sample size. The relationships between binomial dependent variables and multinomial independent variables were analyzed with Cochran Armitage trend test. The relationships between continuous dependent variables and binomial independent variables were analyzed using the T test, or the Wilcoxon rank test, depending on normal vs non-normal distribution of the dependent variables. The relationships between continuous dependent variables and multinomial independent variables were analyzed using the one-way ANOVA test, or the Kruskal Wallis test, depending on normal vs non-normal distribution of the dependent variables. If the tests indicated significant differences among the dependent variable means, then Tukey's post hoc test was used to look at specific differences in the pairs of means. The relationships between continuous dependent variables and continuous independent variables were analyzed using Pearson or Spearman correlation, depending normal vs non-normal distribution of the variables.

Subsequently, the variables were combined into a multivariate model by developing a generalized linear model (including all the independent variables), and then using independent variable selection (Adaptive Lasso with AICc Validation and univariate p-value ≤ 0.20 for inclusion) to

Table 4 Variables and traditional statistical analysis methods

Independent variables	Dependent variables	Statistical analysis
Patient variables	Measured results	
Sex (M: $n=31$/ F: $n=32$)	$C_{surface}$ (Y/N)	Chi square or Fisher's exact
	$X_{c,changed}$% $S_{changed}$%	T test or Wilcoxon rank
Implantation time (months) ($n=59$) Age at removal (years) ($n=63$) BMI ($n=63$)	$C_{surface}$ (Y/N)	T test or Wilcoxon rank
	$X_{c,changed}$% $S_{changed}$%	Pearson or Spearman correlation
Medical variables	Measured results	
Diabetes (Y: $n=16$/ N: $n=46$) Previous hernia repair (Y: $n=44$/ N: $n=18$) Recurrent hernia (Y: $n=52$/ N: $n=3$) Infection (Y: $n=8$/ N: $n=53$) Smoking (Y: $n=4$/ N: $n=59$)	$C_{surface}$ (Y/N)	Chi square or Fisher's exact
	$X_{c,changed}$% $S_{changed}$%	T test or Wilcoxon rank
Surgical variables	Measured results	
Mesh location (intra: $n=24$/extra: $n=38$)	$C_{surface}$ (Y/N)	Chi square or Fisher's exact
	$X_{c,changed}$% $S_{changed}$%	T test or Wilcoxon rank
Mesh variables	Measured results	
Mesh class (Class I: $n=22$, Class II: $n=23$, Class III: $n=18$)	$C_{surface}$ (Y/N)	Cochran Armitage trend
	$X_{c,changed}$% $S_{changed}$%	One Way ANOVA or Kruskal Wallis

determine a reasonable combination of the independent variables that was related to each dependent variable. Using this approach, residuals typically satisfy assumptions for parametric analysis.

All statistical computations were performed using JMP® Pro 14 (SAS Institute Inc, Cary, NC, USA) and α was set at 0.05 for the hypothesis tests.

Results

Forty-six of the 63 FTIR tested mesh samples (73%) exhibited evidence of surface chemical changes. Twenty-one of the 62 DSC tested mesh samples (34%) exhibited crystallinity above or below the pristine control range. Thirty-five of the 35 mechanically tested mesh samples (100%) exhibited changed stiffness behavior compared to pristine control mesh.

Surface degradation characterization

Change in surface chemistry

Forty-six of the 63 tested mesh samples (73%) exhibited evidence of surface chemical changes, including 14 of 22 Class I mesh samples (64%), 18 of 23 Class II mesh samples (78%) and 14 of 18 Class III samples (78%). PP mesh surface chemical changes were independent from mesh class (Cochran Armitage, $p > 0.05$) and not related with patient, surgical, and medical factors (Chi square or Fisher's exact, Wilcoxon rank or T test, $p > 0.05$).

When sublay and intra-peritoneal locations were coded into same group as recoded mesh placement location, $C_{surface}$ was dependent on recoded mesh placement location (univariate, $p = 0.03$) (Fig. 2). Multivariate associations with $C_{surface}$ were evaluated for recoded mesh placement location (univariate, $p = 0.03$) and recurrent hernia (univariate, $p = 0.20$) based on the estimated model selection from all possible combined predictors. Recoded mesh placement location (multivariate, $p = 0.08$) or recurrent hernia (multivariate, $p = 0.22$) did not affect mesh surface degradation (Table 5).

Bulk degradation characterization

Change in crystallinity characterization

Twenty-one of the 62 DSC tested mesh samples (34%) exhibited crystallinity above or below the pristine control range (41.9% to 50.0%) (Fig. 3a). When normalized relative to the crystallinity of pristine mesh, eight of the 62 samples (13%) had $X_{c,changed}$% outside 10% range (Fig. 3b), with an average decrease of 2.5% (SD: 5.1%) (SD: standard deviation) for Class I, increase of 4.1% (SD: 6.0%) for Class II, and increase of 1.8% (SD: 8.4%) for Class III mesh samples (Table 5). Mesh class was a factor affecting changed crystallinity with significantly decreased crystallinity in Class I mesh samples compared to Class II mesh samples (One-way ANOVA with post hoc, $p < 0.01$). Changed crystallinity was also correlated with age at removal (Pearson, $p = 0.03$) but not correlated with other patient, surgical or medical factors (T test, Spearman or Pearson, $p > 0.05$).

Multivariate associations with $X_{c,changed}$% were evaluated for mesh class (univariate, $p = 0.004$), BMI (univariate, $p = 0.15$), and age at removal (univariate, $p = 0.03$) based on the estimated model selection from all possible combined predictors (Table 5). Mesh class was a

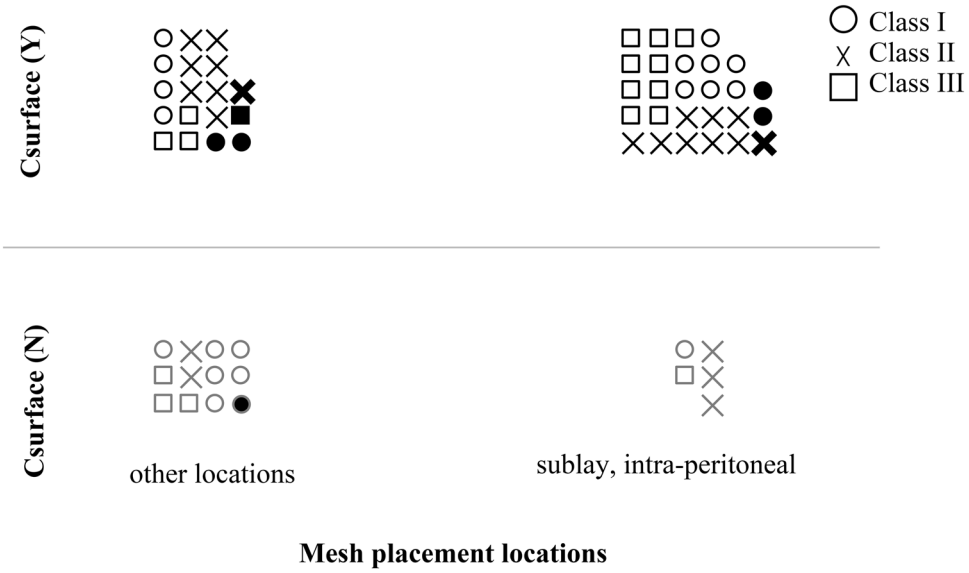

Fig. 2 $C_{surface}$ (Y/N) count distribution ($n = 62$) based on recoded mesh placement location (sublay and intra-peritoneal vs other locations). Each mesh was labeled according to mesh class. Eight mesh samples from infected patients were labeled as bold black

Table 5 Significant univariate and multivariate results from the generalized linear model

Outcome	Univariate models	Mean/Median	*p* Value	Multivariate models	*p* Value
$C_{surface}$	Recoded mesh placement	Dependent	0.03*	Recoded mesh placement	0.08
	Recurrent hernia	Independent	0.20	Recurrent hernia	0.22
$X_{c,changed}$%	Mesh class	$Mean_{class\ I} = (-2.5 \pm 5.1)$ % $Mean_{class\ II} = (4.1 \pm 6.0)$ % $Mean_{class\ III} = (1.8 \pm 8.4)$ %	0.004*	Mesh class	0.008*
	BMI	$r = -0.18$	0.15	BMI	0.24
	Age at removal	$r = 0.27$	0.03*	Age at removal	0.17
$S_{x,changed}$%	Infection	$Mean_{infected} = (-66.7 \pm 13.4)$ % $Mean_{no} = (-36.6 \pm 21.6)$ %	0.01*		
$S_{y,changed}$%	Infection	$Mean_{infected} = (-64.9 \pm 16.1)$ % $Mean_{no} = (-28.1 \pm 25.0)$ %	0.01*		

*$p < 0.05$

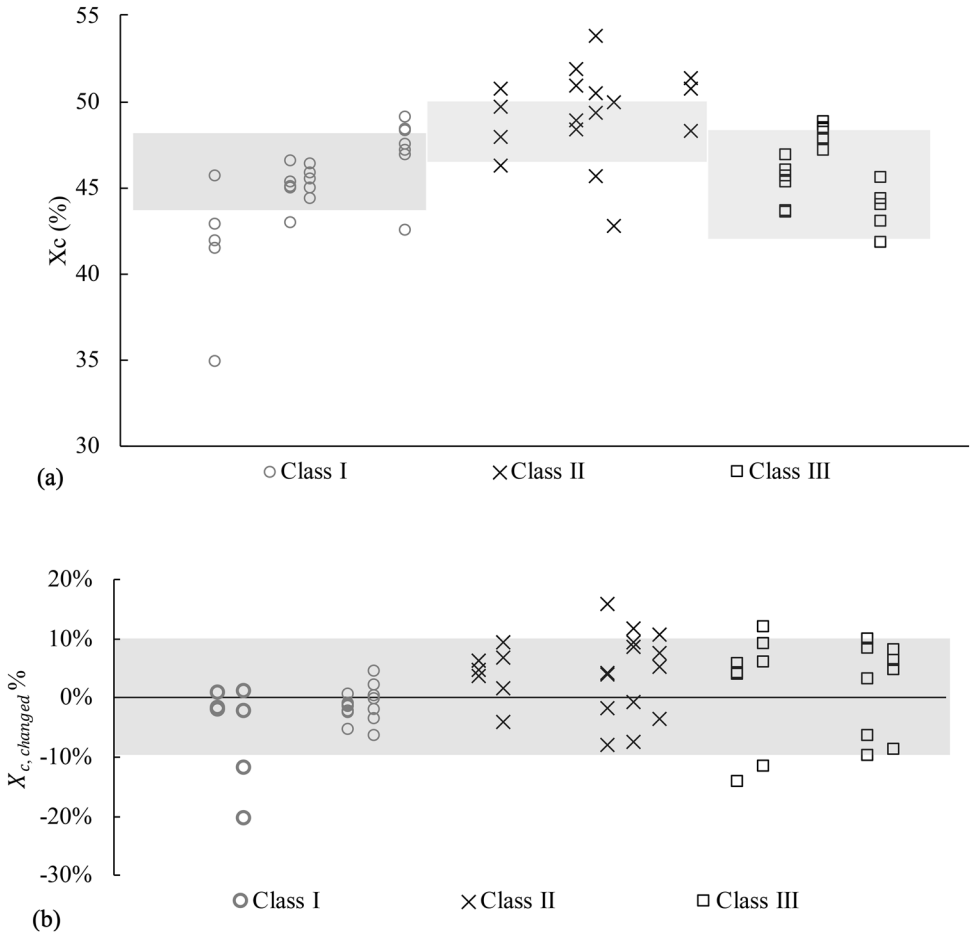

Fig. 3 Results of measured crystallinity (%) and calculated $X_{c,changed}$%. **a** Measured crystallinity of all explanted mesh samples ($n = 62$) grouped in mesh class, compared to pristine controls (shaded area). **b** Normalized percent change in crystallinity ($X_{c,changed}$%) grouped in mesh class, relative to pristine controls. 10% range: shaded area

factor significantly affecting $X_{c,changed}$% (multivariate, $p = 0.008$) while controlling for effects of BMI (multivariate, $p = 0.24$) and age at removal (multivariate, $p = 0.17$). The fit of the estimated model was at r^2 of 0.23.

Change in stiffness

Thirty-five of the 35 mechanically tested mesh samples (100%) exhibited changed stiffness behavior compared to pristine control mesh. The measured stiffness of cleaned

explanted mesh samples ranged from 16.3 to 145.0 N/cm in x direction and from 13.7 to 266.7 N/cm in y direction, compared to the range of pristine controls ranging from 80.7 to 158.5 N/cm in x direction and 134.9 to 265.2 N/cm in y direction (Fig. 4a). When normalized relative to the stiffness of pristine control mesh, $S_{changed}$% ranged from decreased 86.1% (− 86.1%) to decreased 5.5% (− 5.5%) in x direction and decreased 89.8% (− 89.8%) to increased 4.9% (+ 4.9%) in y-direction (Fig. 4b). PP mesh stiffness changes in x- and y-directions were significantly decreased compared to pristine controls (One sample t test, $p < 0.05$).

Mesh samples from infected patients had average $S_{x,changed}$% and $S_{y,changed}$% of -66.7% (SD: 13.4%) and -64.9% (SD: 16.1%), compared to mesh samples from patients without infection averaging $S_{x,changed}$% and $S_{y,changed}$% of -36.6% (SD: 21.6%) and -28.1% (SD: 25.0%) (Fig. 5). Infection was a factor significantly affecting $S_{changed}$% in both x- and y-directions (T test, $p = 0.01$). Changed stiffness was not related with mesh, patient, surgical and other medical factors (One-way ANOVA, T test, Pearson or Spearman, $p > 0.05$). The estimated model of all possible combined predictors for both $S_{x,changed}$% and $S_{y,changed}$% only selected infection for multivariate associations.

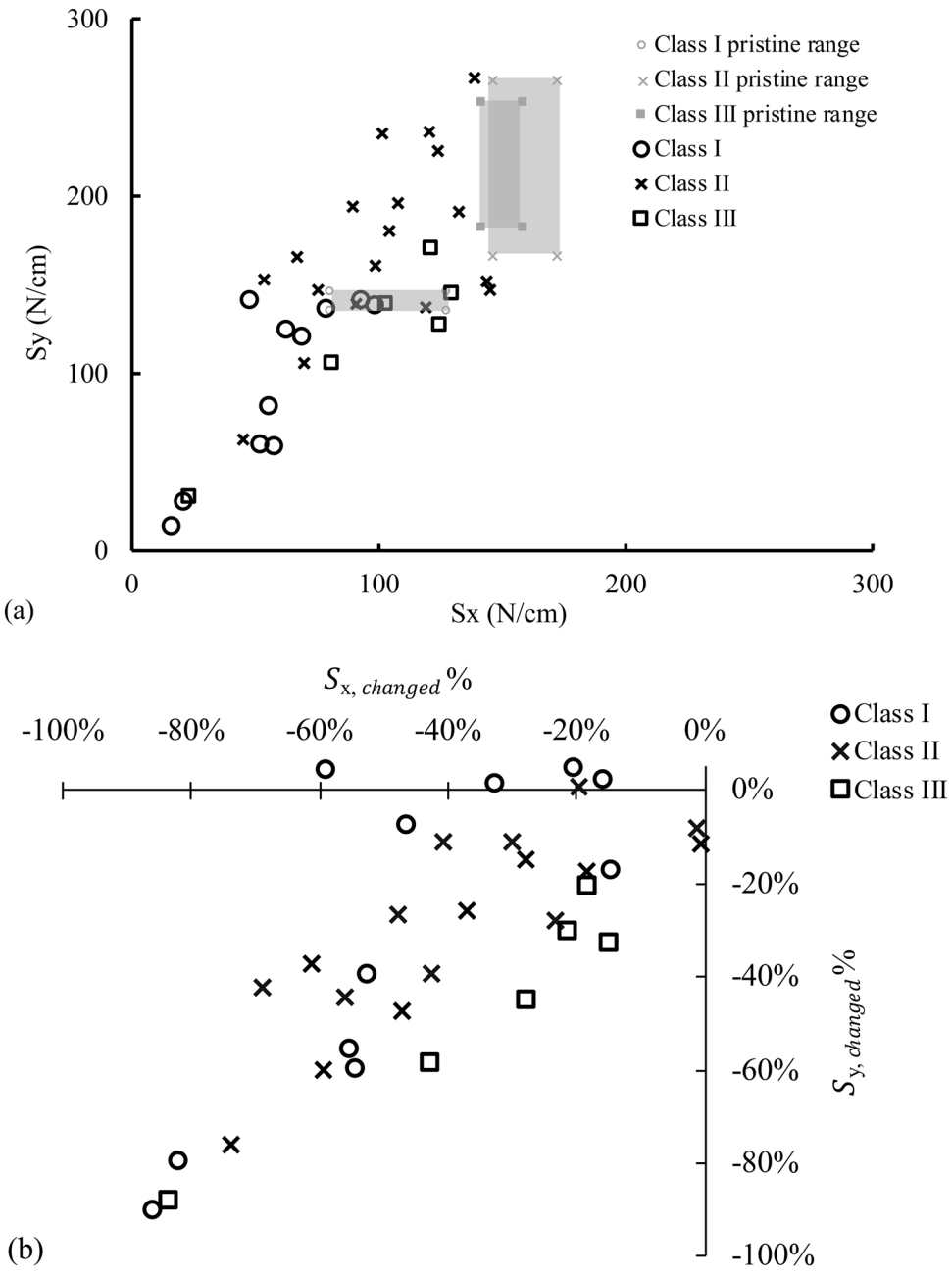

Fig. 4 Results of stiffness (N/cm) and calculated $S_{changed}$%. **a** Stiffness (*Sx* and *Sy*) of all explanted mesh samples ($n = 35$) grouped by mesh class, compared to pristine controls (shaded area). **b** Normalized percent change in stiffness ($S_{changed}$%) grouped by mesh class, relative to pristine controls

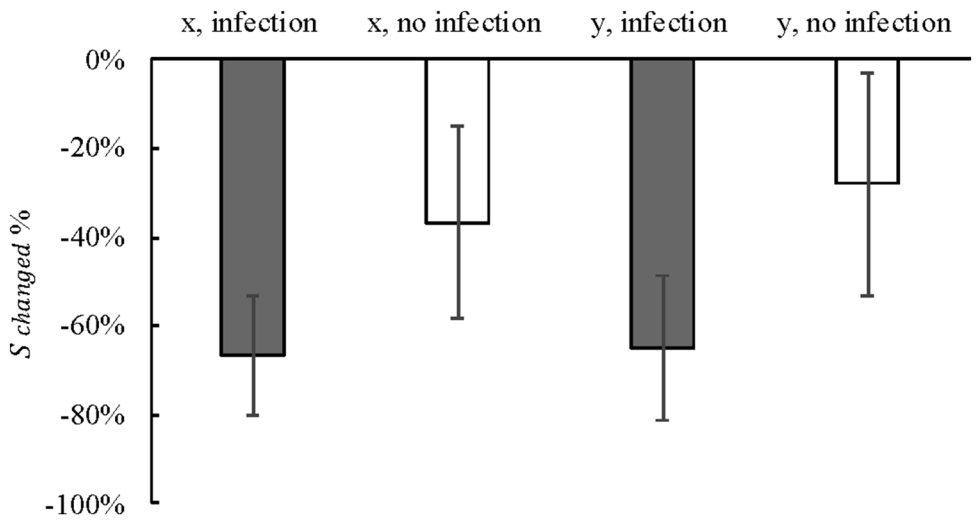

Fig. 5 $S_{changed}$% of mesh samples from infected patients ($n=4$) compared to mesh samples from non-infected patients ($n=30$) in both x and y directions. Infection was a factor significantly affecting $S_{changed}$% (univariate, $p=0.01$)

Relation between surface and bulk degradation

Only 35 explanted mesh samples had data from all three characterization methods (surface chemical change, crystallinity and stiffness). Surface degradation was characterized by detection of surface chemical changes. Bulk degradation was characterized by changes in crystallinity and stiffness. Mesh surface chemical change was not a factor affecting changes of crystallinity or stiffness (T test, $p>0.05$). Twenty-four of the 35 mesh samples (69%) with surface degradation had median $X_{c,changed}$% of + 4.6%, compared to + 3.1% of the 11 mesh samples without surface degradation. Mesh samples with surface degradation had average $S_{x,changed}$% and $S_{y,changed}$% of − 43.2% (SD: 22.5%) and − 36.2% (SD: 24.6%), compared to − 35.3% (SD: 23.5%) and − 24.7% (SD: 29.6%) of mesh samples without surface degradation. The changed crystallinity was not correlated with the changed stiffness (Pearson, $p>0.05$).

Discussion

This study explored mechanisms potentially contributing to PP mesh degradation using 63 explanted PP mesh samples with documentation of basic patient demographics, clinical history and details of mesh structures. The material changes were characterized using surface chemistry changes, crystallinity changes, and stiffness changes consistent with chemical and physical markers cited as evidence of in vivo PP degradation in previous studies [6, 12–15]. Compared to pristine control samples, subsets of mesh explants had evidence of surface oxidation, altered crystallinity, or changed mechanical properties. The findings in this study supported the proposed hypotheses that: (1) infection was a factor affecting stiffness changes; (2) mesh with small pore size (mesh class) was a factor affecting crystallinity changes normalized to pristine controls. However, the study failed to support the hypotheses that: 1) infection was a factor affecting surface chemistry changes and crystallinity changes; (2) mesh class was a factor affecting surface chemistry changes and stiffness changes; (3) mesh placement location was a factor affecting PP material changes.

Multivariable associations used an estimated model to evaluate the significant impact of certain independent predictors on PP mesh material changes when combining all possible predictors [41]. This study confirmed the significant impact of mesh class for changes in crystallinity ($X_{c,changed}$%) when combining all possible predictors (Table 5), consistent with other in vitro and in vivo studies [5, 42, 43]. Mesh class significantly affected $X_{c,changed}$% in both univariate (univariate, $p=0.004$) and multivariate analysis (multivariate, $p=0.008$), indicating crystallinity stability was determined by mesh class even with consideration of all possible predictors. This study used $X_{c,changed}$% instead of Xc due to the different measured crystallinity of pristine meshes ranging from 41.9 to 50.0% (Fig. 3), determined by manufacturers [5, 42]. As to surface oxidation ($C_{surface}$), although there was a trend for PP mesh surface oxidation when mesh implanted in sublay and intra-peritoneal location (univariate, $p=0.03$) (Fig. 2), $C_{surface}$ was independent on mesh implantation location in estimated model (multivariate, $p=0.08$) (Table 5), indicating $C_{surface}$ was not associated with any specific predictor when considering all possible predictors. As to changes in mesh stiffness ($S_{changed}$%), although infection was a significant factor for $S_{x,changed}$% and $S_{y,changed}$% (univariate, $p=0.01$), it was unable to be analyzed in multivariate associations (Table 5), possibly due to the small sample size of only four mesh samples from infected patients, compared to 31 mesh samples from non-infected patients.

Evaluating explanted PP mesh material changes and their associations with clinical characteristics is important to predict the risk factors on PP mesh degradation. In this study,

46 of 63 explanted mesh samples (73%) had evidence of PP mesh surface chemistry changes (Fig. 2), but only eight of 62 explanted mesh samples (13%) had normalized crystallinity changes greater than 10% range, compared to pristine controls (Fig. 3b). Regardless of the material changes noted, none of the explanted mesh had evidence of gross mesh rupture while in clinical use. Due to the small number of explanted mesh with evidence of material changes, it was not possible to discern whether the material changes had any impact on the clinical factors.

Evidence of polymer oxidation has occurred in other implanted polymeric biomaterials and is linked to exposure to mechanical stress or an oxidizing environment [44]. In this study of explanted PP hernia mesh, there was evidence of surface chemical changes consistent with oxidation (46 of 63, 73%) and altered crystallinity (21 of 62, 34%). These results are similar to the 49% incidence reported for explanted PP pelvic floor mesh [16]. Therefore, it is useful to consider known mechanisms contributing to chemical changes in pelvic floor mesh explants while recognizing differences between the physiological environments in the abdominal wall and pelvic floor. Different from meshes implanted in the abdomen, pelvic floor surgical meshes are exposed to higher tension and have relatively greater risk of exposure to bacteria from the outside environment [21], resulting in higher mechanical strains and accumulation of ROS due to bacterial adherence. The estimated static loads on implanted pelvic mesh are 10.5–15.5 N/cm, compared to loads of 7.5 N/cm for implanted hernia mesh [21]. Pelvic surgical mesh degradation tends to occur due to the polymer chain scission induced by mechanical strains or the infusion of ROS, and further studies are needed to determine if similar mechanisms exist in hernia mesh [16, 21].

Rigorous attention to mesh cleaning is critical to avoid false observation of mesh surface oxidation associated with ineffective cleaning [10]. The current study used a 10-step modified cleaning protocol (Table 3) and repeated cleaning cycles to avoid interference with subsequent analysis methods. The use of enzymatic solutions instead of sodium chloride to remove tissues reduced the risk of oxidative residues due to sodium chloride exposure [5, 45]. The repeated use of enzymatic solutions assisted removing adhered proteins [10], caused by protein adsorption on the PP mesh surface after implantation [46]. The use of fresh frozen explanted PP mesh instead of formalin-fixed explanted PP mesh eliminated the formalin-fixed proteins strongly adhered to the mesh surface due to the chemical process of fixative crosslinking [3, 10, 16]. Formalin-fixed proteins can have a morphology similar to PP surface cracking, which is difficult to distinguish from PP degradation under scanning electron microscopy (SEM) [10]. The current study used FTIR to precisely distinguish adhered proteins and PP surface oxidation (Fig. 1a), avoiding false observation of mesh surface cracking with SEM [9–11].

Several limitations are noted. (1) Due to the nature of implant retrieval analysis after revision surgery [45], patient selection to control the clinical and surgical factors was not possible and it was unknown if these findings can be generalized to a broader population. (2) Due to the relative short implantation time (median 24 months), material changes expected for longer in vivo durations should not be extrapolated from the reported data. (3) It was difficult to generalize the relationship between infection and material changes due to the small number of infection cases. (4) There was limited documentation of mesh selection at index surgery and it was unknown whether the PP mesh had absorbable components or fibers containing antioxidants. Antioxidants can alter the surface chemistry changes caused by infection or chemicals in peritoneal fluid, compared to PP monofilaments without antioxidants [3, 10]. In vivo resorption of absorbable components in PP mesh can reduce mesh stiffness (Fig. 4) [47] compared to mesh without absorbable component [3, 5, 43], interfering with the observation of monofilament PP mesh stiffness changes in the current study. Such in vivo resorption also increased the difficulty of identifying mesh types due to the same mesh structure used for mesh with and without absorbable component. For example, the absorbance of PDS/oxidized cellulose in Proceed® results in same mesh structure and same chemistry as Prolene® Soft.

There is a need for direct measurement of ROS in vivo to explore the proposed PP mesh degradation mechanism involving ROS accumulation, which are capable of PP radical scission [3, 5]. In cases of infection, the immune response triggers ROS release to attack bacteria by reacting with organic molecules [17, 48–50], but ROS also exist in the process of wound healing to induce vascular endothelial growth factor expression [51] and the formation of peritoneal tissue adhesion [52]. In the current study, 88% of mesh samples from infected cases and 70% of mesh sample from non-infected patients had surface oxidation (Fig. 2), which supports the presence of ROS in both patient subsets, according to the results from other in vitro studies [5, 19]. The direct measurement of ROS [17] would assist more precise categorization of the current in vivo dataset.

Similarly, there is a need for estimating in vivo mechanical strains on mesh to explore the proposed PP mesh degradation mechanism involving mechanical strains in the mesh, which are capable of increasing localized stress and causing polymer chain scission [7, 12, 20, 21]. Mechanical strains in mesh can be influenced by fibrous capsulation or scar formation [21], excess abdominal adipose tissues [53], and altered wound healing process due to diabetes or smoking [53]. Mechanical strains induced by the same applied tension magnitude can also vary due to mesh knitting structures [35],

as confirmed by the different stiffness ranges for pristine control mesh of different mesh classes (Fig. 4a). Although the current study analyzed the associations between measured material changes and comorbidities (Table 5), such as BMI, diabetes, smoking status, the findings could not reflect the impact of quantified mechanical strains on PP mesh degradation. The direct measurement of mechanical strains [54] could assist statistical correlation of mesh degradation and material changes.

Conclusion

Highly variable in vivo conditions expose mesh to mechanisms that alter clinical outcomes and potentially contribute to mesh degradation. These PP mesh explants after 0.5 to 13 years in vivo had measurable changes in surface chemistry, crystallinity and mechanical properties, with significant trends associated with factors of mesh placement, mesh class, and infection. Using multivariate statistical approach to control for clinical characteristics, infection was a significant factor affecting mesh stiffness changes and mesh class was a significant factor affecting PP crystallinity changes. However, direct measures of ROS concentrations in the peritoneal fluid before retrieval surgery are needed to generate a direct relationship between ROS concentrations and mesh material changes. This relationship would provide an estimate of the severity of the inflammatory response and potential mesh material changes during in vivo exposure in patients. Given that mesh structures and mesh materials are commonly modified by manufacturers or removed entirely from the market, it is recommended that material properties for pristine meshes implanted in patients should be regularly measured and reported using standard methods.

Funding This work was supported by National Institutes of Health Grant P20GM121342.

Declarations

Disclosures Dr. Melinda Harman has received funding related to other research on hernia repair from NIH STTR 1R41DK120168-01 and the Clemson University Research Foundation. Dr. B. Todd Heniford has received payment or honoraria for educational activities and events from WL Gore and Allergan, payment for expert testimony, and he participates on a data safety monitoring/advisory board for Allergan. Dr. Vedra Augenstein has received Grants or contracts from W.L. Gore and Allergan and has received consulting fees from Allergan, 3M-KCI, Meditorin, CR Bard, Intuitive Surgical, and Vicarious Surgical. Dr. Xinyue Lu, Dr. Melinda Harman, Ms. Brittney McIver, and Dr. William Bridges have no other conflicts of interest or financial ties to disclose.

References

1. Simons MP, Aufenacker T, Bay-Nielsen M, Bouillot JL, Campanelli G, Conze J, de Lange D, Fortelny R, Heikkinen T, Kingsnorth A, Kukleta J, Morales-Conde S, Nordin P, Schumpelick V, Smedberg S, Smietanski M, Weber G, Miserez M (2009) European Hernia Society guidelines on the treatment of inguinal hernia in adult patients. Hernia 13(4):343–403
2. Graham J, Usher FC, Perry JL, Barkley HT (1960) Marlex mesh as a prosthesis in the repair of thoracic wall defects. Ann Surg 151(4):469–479
3. Liebert TC, Chartoff RP, Cosgrove SL, Mccuskey RS (1976) Subcutaneous implants of polypropylene filaments. J Biomed Mater Res 10(6):939–951
4. Mary C, Marois Y, King MW, Laroche G, Douville Y, Martin L, Guidoin R (1998) Comparison of the *in vivo* behavior of polyvinylidene fluoride and polypropylene sutures used in vascular surgery. Asaio J 44(3):199–206
5. Gil D, Rex J, Reukov V, Vertegel A (2018) *In vitro* study on the deterioration of polypropylene hernia repair meshes. J Biomed Mater Res B 106(6):2225–2234
6. Iakovlev VV, Guelcher SA, Bendavid R (2017) Degradation of polypropylene *in vivo*: a microscopic analysis of meshes explanted from patients. J Biomed Mater Res B 105(2):237–248
7. Rynkevic R, Martins P, Pereira F, Ramião N, Fernandes AA (2017) *In vitro* study of the mechanical performance of hernia mesh under cyclic loading. J Mater Sci Mater Med 28(11):1–7
8. Imel A, Malmgren T, Dadmun M, Gido S, Mays J (2015) *In vivo* oxidative degradation of polypropylene pelvic mesh. Biomaterials 73:131–141
9. Thompson M, Guelcher S, Bendavid R, Iakovlev V, Ostergard DR (2017) *In vivo* polypropylene mesh degradation is hardly a myth. Int Urogynecol J 28(2):333–335
10. Thames SF, White JB, Ong KL (2017) The myth: *in vivo* degradation of polypropylene-based meshes. Int Urogynecol J 28(2):285–297
11. Thames SF, Thames SF, White JB, White JB, Ong KL, Ong KL (2017) Reply to "*In vivo* polypropylene mesh degradation is hardly a myth". Int Urogynecol J 28(2):337–338
12. Wood AJ, Cozad MJ, Grant DA, Ostdiek AM, Bachman SL, Grant SA (2013) Materials characterization and histological analysis of explanted polypropylene, PTFE, and PET hernia meshes from an individual patient. J Mater Sci Mater Med 24(4):1113–1122
13. Coda A, Bendavid R, Botto-Micca F, Bossotti M, Bona A (2003) Structural alterations of prosthetic meshes in humans. Hernia 7(1):29–34
14. Ostergard DR (2011) Degradation, infection and heat effects on polypropylene mesh for pelvic implantation: what was known and when it was known. Int Urogynecol J 22(7):771–774
15. Costello CR, Bachman SL, Grant SA, Cleveland DS, Loy TS, Ramshaw BJ (2007) Characterization of heavyweight and lightweight polypropylene prosthetic mesh explants from a single patient. Surg Innov 14(3):168–176
16. Clavé A, Yahi H, Hammou J, Montanari S, Gounon P, Clavé H (2010) Polypropylene as a reinforcement in pelvic surgery is not inert: comparative analysis of 100 explants. Int Urogynecol J 21(3):261–270
17. Bardon J, Lukaszewicz A, Faivre V, Huot B, Payen D (2016) Reactive oxygen species measure for rapid detection of infection in fluids. Ann Intensive Care 6(1):1–8
18. Ratner BD, Hoffman AS, Schoen FJ, Lemons JE (2013) Biomaterials science: an introduction to materials in medicine. Academic Press, pp. 179–194.

19. Talley AD, Rogers BR, Iakovlev V, Dunn RF, Guelcher SA (2017) Oxidation and degradation of polypropylene transvaginal mesh. Biomater Sci Polym Ed 28(5):444–458
20. Li X, Kruger JA, Jor JWY, Wong V, Dietz HP, Nash MP, Nielsen PM (2014) Characterizing the ex vivo mechanical properties of synthetic polypropylene surgical mesh. J Mech Behav Biomed Mater 37:48–55
21. Taylor D (2018) The failure of polypropylene surgical mesh *in vivo*. J Mech Behav Biomed Mater 88:370–376
22. Klinge U, Klosterhalfen B, Müller M, Ottinger AP, Schumpelick V (1998) Shrinking of polypropylene mesh *in vivo*: an experimental study in dogs. Eur J Surg 164(12):965–969
23. Capobianco A, Cottone L, Monno A, Manfredi AA, Rovere-Querini P (2017) The peritoneum: healing, immunity, and diseases. J Pathol 243(2):137–147
24. Bedaiwy MA, Falcone T (2003) Peritoneal fluid environment in endometriosis. Clinicopathological implications. Minerva Ginecol 55(4):333–345
25. Schlosser KA, Maloney SR, Gbozah K, Prasad T, Colavita PD, Augenstein VA, Heniford BT (2020) The impact of weight change on intra-abdominal and hernia volumes. Surgery 167(5):876–882
26. Cox TC, Blair LJ, Huntington CR, Colavita PD, Prasad T, Lincourt AE, Heniford BT, Augenstein VA (2016) The cost of preventable comorbidities on wound complications in open ventral hernia repair. J Surg Res 206(1):214–222
27. Huntington C, Gamble J, Blair L, Cox T, Prasad T, Lincourt A, Augenstein VA, Heniford BT (2016) Quantification of the effect of diabetes mellitus on ventral hernia repair: results from two national registries. Am Surg 82(8):661–671
28. Heniford BT, Ross SW, Wormer BA, Walters AL, Lincourt AE, Colavita PD, Kercher KW, Augenstein VA (2020) Preperitoneal ventral hernia repair: a decade long prospective observational study with analysis of 1023 patient outcomes. Ann Surg 271(2):364–374
29. Lake SP, Ray S, Zihni AM, Thompson DM Jr, Gluckstein J, Deeken CR (2015) Pore size and pore shape – but not mesh density – alter the mechanical strength of tissue ingrowth and host tissue response to synthetic mesh materials in a porcine model of ventral hernia repair. J Mech Behav Biomed Mater 42:186–197
30. Klinge U, Klosterhalfen B, Birkenhauer V, Junge K, Conze J, Schumpelick V (2002) Impact of polymer pore size on the interface scar formation in a rat model. J Surg Res 103(2):208–214
31. Klosterhalfen B, Klinge U (2013) Retrieval study at 623 human mesh explants made of polypropylene - impact of mesh class and indication for mesh removal on tissue reaction. J Biomed Mater Res B 101(8):1393–1399
32. Klosterhalfen B, Junge K, Klinge U (2005) The lightweight and large porous mesh concept for hernia repair. Expert Rev Med Devices 2(1):103–117
33. Klinge U, Park J, Klosterhalfen B (2013) The ideal mesh? Pathobiology 80(4):169
34. Weyhe D, Cobb W, Lecuivre J, Alves A, Ladet S, Lomanto D, Bayon Y (2015) Large pore size and controlled mesh elongation are relevant predictors for mesh integration quality and low shrinkage–systematic analysis of key parameters of meshes in a novel minipig hernia model. Int J Surg 22:46–53
35. Deeken CR, Thompson J, Dominic M, Castile RM, Lake SP (2014) Biaxial analysis of synthetic scaffolds for hernia repair demonstrates variability in mechanical anisotropy, non-linearity and hysteresis. J Mech Behav Biomed 38:6–16
36. Casey EM (2015) Physical characterization of surgical mesh after function in hernia repair. All Theses. 2085.
37. Halligan S, Parker SG, Plumb AA, Windsor ACJ (2018) Imaging complex ventral hernias, their surgical repair, and their complications. Eur Radiol 28(8):3560–3569
38. Klinge U, Klosterhalfen B (2012) Modified classification of surgical meshes for hernia repair based on the analyses of 1000 explanted meshes. Hernia 16(3):251–258
39. Gil D (2017) Naturally derived anti-inflammatory and antibacterial coatings for surgical implants. All Dissertations. 2067.
40. Patel HN, Garcia R, Schindler C, Dean D, Pogwizd SM, Singh R, Vohra YK, Thomas V (2015) Fibro-porous poliglecaprone/polycaprolactone conduits: synergistic effect of composition and *in vitro* degradation on mechanical properties. Polym Int 64(4):547–555
41. Cavallo JA, Roma AA, Jasielec MS, Ousley J, Creamer J, Pichert MD, Baalman S, Frisella MM, Matthews BD, Deeken CR (2014) Remodeling characteristics and collagen distribution in synthetic mesh materials explanted from human subjects after abdominal wall reconstruction: an analysis of remodeling characteristics by patient risk factors and surgical site classifications. Surg Endosc 28(6):1852–1865
42. Afonso JS, Jorge R, Martins PS, Soldi MD, Alves OL, Patricio B, Mascarenhas T, Sartori MG, Girao MJ (2009) Structural and thermal properties of polypropylene mesh used in treatment of stress urinary incontinence. Acta Bioeng Biomech 11(3):27–33
43. Costello CR, Bachman SL, Ramshaw BJ, Grant SA (2007) Materials characterization of explanted polypropylene hernia meshes. J Biomed Mater Res B 83B(1):44–49
44. Currier BH, Van Citters DW, Currier JH, Carlson EM, Tibbo ME, Collier JP (2013) *In vivo* oxidation in retrieved highly crosslinked tibial inserts. J Biomed Mater Res B 101B(3):441–448
45. Zhang Z, Guidoin R, King MW, How TV, Marois Y, Laroche G (1995) Removing fresh tissue from explanted polyurethane prostheses - which approach facilitates physicochemical analysis. Biomaterials 16(5):369–380
46. Hlady V, Buijs J (1996) Protein adsorption on solid surfaces. Curr Opin Biotechnol 7(1):72–77
47. Cobb WS, Burns JM, Peindl RD, Carbonell AM, Matthews BD, Kercher KW, Heniford BT (2006) Textile analysis of heavy weight, mid-weight, and light weight polypropylene mesh in a porcine ventral hernia model. J Surg Res 136(1):1–7
48. Heinzelmann M, Simmen HP, Battaglia H, Friedl HP, Trentz O (1997) Inflammatory response after abdominal trauma, infection, or intestinal obstruction measured by oxygen radical production in peritoneal fluid. Am J Surg 174(4):445–447
49. Kolaczkowska E, Kubes P (2013) Neutrophil recruitment and function in health and inflammation. Nat Rev Immunol 13(3):159–175
50. Segal AW (2005) How neutrophils kill microbes. Annu Rev Immunol 23(1):197–223
51. Sen CK, Khanna S, Babior BM, Hunt TK, Ellison EC, Roy S (2002) Oxidant-induced vascular endothelial growth factor expression in human keratinocytes and cutaneous wound healing. J Biol Chem 277(36):33284–33290
52. Roy S, Clark CJ, Mohebali K, Bhatt U, Wallace WA, Nahman NS, Nahman NS, Ellison EC, Melvin WS, Sen CK (2004) Reactive oxygen species and egr-1 gene expression in surgical postoperative peritoneal adhesions. World J Surg 28(3):316–320
53. Novitsky YW, Orenstein SB (2013) Effect of patient and hospital characteristics on outcomes of elective ventral hernia repair in the United States. Hernia 17(5):639–645
54. Kuehnert N, Kraemer NA, Otto J, Donker HCW, Slabu I, Baumann M, Kuhl CK, Klinge U (2011) *In vivo* MRI visualization of mesh shrinkage using surgical implants loaded with superparamagnetic iron oxides. Surg Endosc 26(5):1468–1475

Publisher's Note Springer Nature remains neutral with regard to jurisdictional claims in published maps and institutional affiliations.